Wave Function Intensity Statistics from Unstable Periodic Orbits

L. Kaplan*

Department of Physics and Society of Fellows, Harvard University, Cambridge, Massachusetts 02138

(Received 5 November 1997)

We examine the effect of short unstable periodic orbits on wave function statistics in a classically chaotic system, and find that the tail of the wave function intensity distribution in phase space is dominated by scarring associated with the least unstable periodic orbits. In an ensemble average over systems with classical orbits of different instabilities, a power-law tail is found, in sharp contrast to the exponential prediction of random matrix theory. The calculations are compared with numerical data, and quantitative agreement is obtained. [S0031-9007(98)05543-4]

PACS numbers: 05.45.+b, 03.65.Sq

Quantum eigenstates of classically chaotic systems generically exhibit a phenomenon known as scarring, the enhancement of intensity along short unstable periodic orbits for some fraction of the wave functions. Scarring is a fascinating example of the influence of identifiable classical structures on stationary quantum properties and on long-time quantum transport in a classically ergodic system. The occurrence of scars is in some sense paradoxical, because classically, all such short-time information is destroyed at long times, and a classical probability distribution after being evolved for a sufficiently long time retains no memory of its initial state. Scarring is one of the most dramatic examples of a departure of quantum chaotic systems from the predictions of random matrix theory (RMT), according to which wave functions must be evenly distributed over phase space, up to quantum fluctuations. Scarring has now been observed experimentally in a variety of systems, including microwave cavities [1,2], tunnel junctions [3], and the hydrogen atom in a uniform magnetic field [4,5].

Examples of scarring were observed numerically in [6], and a theory based on the semiclassical evolution of Husimi states near a periodic orbit was provided. Later work by Bogomolny [7] and Berry [8] involved calculations in coordinate space and Wigner phase space, respectively. All these works were based on the linearized dynamics around the unstable periodic orbit, and were thus, by construction, theories of the short-time behavior only. Yet to get a true understanding of the properties of individual eigenstates it is essential to understand the long-time quantum dynamics, including returns of amplitude to the original periodic orbit after undergoing excursions into other areas of phase space. In a recent paper [9], a formalism was developed for dealing with these nonlinear contributions to scarring, providing quantitative agreement of the theory with numerical results. This work used a measure of scarring based on Husimi intensities. (Recently Fishman, Agam, and others have provided interesting new perspectives on the problem of scarring, and have offered a measure of scarring related to, but somewhat different from ours [10]. A number of other authors have also made significant contributions in this area; we cannot list them all but a few recent references are provided in [11].) In this paper, we will apply a result previously obtained in [9] to compute the effect of scarring on the wave function intensity distribution, a function which has been investigated previously for diffusive systems [12].

We first give a general idea of the formalism and state the key result of [9] which is relevant to the present work. A Gaussian wave packet $|\Psi\rangle$ is initially centered close to a classical periodic orbit and allowed to evolve. If the instability exponent λ of the orbit is small, the function $A(t) = \langle\Psi|\Psi(t)\rangle$ will (under the linearized dynamics) exhibit recurrences on a time scale of one period T_P, and the amplitude of these recurrences decays on a scale T_P/λ. This decay leads to the formation of envelopes in the local density of states $S(E)$, which is the Fourier transform of the autocorrelation function. These envelopes in the energy spectrum have spacing $\hbar/T_P$, width scaling as $\hbar\lambda/T_P$ for small λ, and height scaling as λ^{-1}. Long-time (nonlinear) recurrences lead to fluctuations multiplying this envelope in the energy domain. Eventually, by the Heisenberg time $T_H = \hbar/\Delta$, where Δ is the mean level spacing, individual peaks are resolved in the spectrum $S(E)$, the heights of the peaks being the intensities of the corresponding eigenstates at the test state $|\Psi\rangle$, $S(E) = \sum_n |\langle n|\Psi\rangle|^2 \delta(E - E_n)$.

The simplest picture of the nonlinear recurrences assumes that the periods, actions, and homoclinic points corresponding to the long-time excursions are random and uncorrelated, up to the constraint of unitarity which produces delta-function spectral peaks by the Heisenberg time. This, when combined with the known short-time dynamics in the linear regime, can be shown to produce a chi-squared distribution of spectral intensities multiplying the original linear envelope.

[Strong, isolated nonlinear recurrences which cannot be treated statistically, as well as correlations between long-time excursions modify this simple picture. However, we will find that for the generalized baker's maps (a paradigmatic example of hard chaos), the assumptions of randomness beyond the linear decay time lead to results which are in quite reasonable agreement with numerical data.]

 0031-9007/98/80(12)/2582(4)$15.00

A key result of the calculations in Ref. [9] is the following: *Individual spectral lines (overlap intensities) in the local density of states obey the usual chi-squared (Porter-Thomas) fluctuations, but these are modulated by the Fourier transform of the linearized short-time autocorrelation function.* The latter can be computed analytically in terms of the instability λ of the classical orbit in question [see Eq. (4) below]. More explicitly, in the case of complex eigenstates, the chi-squared distribution has 2 degrees of freedom, and in the absence of scarring the probability of having a spectral line height greater than x is given by $P(x) = \exp(-x)$. Here x is normalized to have a mean value of unity, i.e., $x_n = N|\langle n|\Psi\rangle|^2$, where N is the total number of states. Now in the presence of scarring this is modified to

$$P(E, x) = \exp[-x/S_{\rm lin}(E)] \tag{1}$$

for an eigenstate with energy E. *Here $S_{\rm lin}$ is the spectral envelope given by the Fourier transform of the linearized dynamics* [Eq. (4) for the case treated in the present paper].

In the following discussion we will for simplicity consider the case of scarring by a fixed point of a discrete-time map. (The generalization of the results to orbits of period greater than one and to continuous time systems is straightforward [9].) So let us consider without loss of generality a hyperbolic fixed point at the origin of a compact phase space, with exponent λ, and stable and unstable manifolds oriented along the p and q axes, respectively. The equations of motion near the fixed point are then given by

$$\begin{aligned} q' &= q\exp(\lambda t)\,, \\ p' &= p\exp(-\lambda t)\,. \end{aligned} \tag{2}$$

In the presence of shearing, e.g., $\partial q'/\partial p \neq 0$, or for nonorthogonal stable and unstable manifolds, or in the case where the manifolds are not oriented along the p and q axes, a canonical transformation would first need to be performed to get the equations of motion into the form above. Now we define our test state to be a Gaussian wave packet centered at (q_0, p_0), with horizontal width σ and vertical width $\sigma_p = \hbar/\sigma$. In coordinate representation this is given by

$$\Psi(q) = (4\pi\sigma_p^2)^{1/4}\exp[-(q - q_0)^2/2\sigma^2 + ip_0(q - q_0)/\hbar]. \tag{3}$$

In situations described above where the local equations of motion do not have the form of Eq. (2) in the natural coordinates, an optimal test state would have a complex width σ in those coordinates, as can be seen by performing a canonical transformation of the Gaussian of Eq. (3).

We now allow the wave packet to evolve under the linearized dynamics, stretching each time step by a factor of e^{λ} in the q direction and shrinking by the same factor in the p direction. The linearized quantum autocorrelation function after time t is given by

$$A_{\rm lin}(q, p, \sigma, \lambda, t) = \frac{\exp i\theta_0 t}{\cosh\lambda t} \times \exp\left[-\frac{\cosh\lambda t - 1}{2\cosh\lambda t}\left(\frac{q_0^2}{\sigma^2} + \frac{p_0^2}{\sigma_p^2}\right) - \frac{iqp}{\hbar}\tanh\lambda t\right]. \tag{4}$$

Here θ_0 is the phase associated with one iteration of the periodic orbit, given by the classical action in units of $\hbar$, plus any Maslov indices associated with caustics in the classical dynamics. θ_0 determines the location of the peak in the spectral envelope $S_{\rm lin}(E)$, defined to be the Fourier transform of $A_{\rm lin}(t)$. Since we will be interested in performing an energy average, we freely set $\theta_0 = 0$.

Now the expression in Eq. (4) can be inserted into Eq. (1) to obtain the distribution of wave function intensities at a given energy. Because we wish here to consider all eigenstates, independent of energy, we then perform an energy averaging, remembering that for a map the quasienergy is defined to lie between 0 and 2π only. We also notice that the tail of the intensity distribution will be dominated by the peak of the spectral envelope at $E = 0$, and we therefore can use a saddle-point approximation, obtaining

$$\begin{aligned} P(q, p, \sigma, \lambda, x) &= \frac{1}{2\pi}\int dE\, P(q, p, \sigma, \lambda, E, x) \\ &\approx \frac{1}{\sqrt{2\pi}}\,\frac{\exp[-x/S_{\rm lin}(q, p, \sigma, \lambda, E = 0)]}{\sqrt{\frac{-x}{S_{\rm lin}(0)^2}\,\frac{\partial^2 S_{\rm lin}}{\partial E^2}}}\,, \end{aligned} \tag{5}$$

where the expression obtained is an asymptotic form valid for large x. For small λ, the sum over time steps can be replaced by an integral, and we have at $q_0 = p_0 = 0$

$$S_{\rm lin}(E) = \int dt\,\frac{e^{-iEt}}{\sqrt{\cosh\lambda t}}\,. \tag{6}$$

Now by dimensional analysis, $S_{\rm lin}(0) = Q/\lambda$ and $\frac{\partial^2 S_{\rm lin}}{\partial E^2}(0) = -W/\lambda^3$, where Q and W are numerical constants. We thus obtain the first result of this paper, the tail of the intensity distribution for a wave packet centered on a periodic orbit,

$$P(q_0 = 0, p_0 = 0, \sigma, \lambda, x) = \frac{1}{\sqrt{2\pi}}\,\frac{Q}{\sqrt{W}}\,\lambda(x\lambda)^{-1/2}e^{-x\lambda/Q}. \tag{7}$$

Notice that the exponential tail has been effectively stretched by a factor of Q/λ, corresponding to the increased height of the peak of the linear envelope at small λ. There is also a linear suppression factor of λ, corresponding to the width of the peak in $S_{\rm lin}(E)$, and indicating that only a fraction scaling as λ of all the eigenstates are effectively scarred. The remainder of the eigenstates are typically "antiscarred," having on average a lower intensity at the periodic orbit than would be expected based on RMT. This distribution will have a

nontrivial inverse participation ratio (IPR), scaling as the inverse of the width of the linear envelope, i.e., as $1/\lambda$.

The region of validity of Eq. (7) is

$$1 \ll \lambda^{-1} \ll x \ll N . \tag{8}$$

The first inequality ensures that many iterations of the periodic orbit contribute (so the sum over iterations can be replaced by an integral) and the scarring is strong. In fact, however, because of the large value of the numerical constant Q, the formula works well even for exponents as small as $\ln 2$, as will be seen in the numerical study below. The second inequality says that we are in the tail of the distribution and the events are all coming from the peak of the linear envelope. The third inequality is a unitarity constraint—obviously our assumption of random fluctuations breaks down for intensities of order unity, when the entire wave function would be concentrated in a phase space area of order $\hbar$.

Now we go on to perform a similar analysis integrating over the phase space variables q_0 and p_0. As before, we take the exponential $\exp[-x/S_{\rm lin}(q_0, p_0, \ldots)]$ and expand to second order in q_0, p_0 around the maximum $q_0 = p_0 = 0$. Then upon integration by stationary phase we pick up a determinant factor of

$$\frac{2\pi[S_{\rm lin}(0)]^2}{x} \frac{1}{\sqrt{\frac{\partial^2 S_{\rm lin}}{\partial q_0^2} \frac{\partial^2 S_{\rm lin}}{\partial p_0^2}}} . \tag{9}$$

Here we have taken the classical phase space volume to be unity for simplicity. Now for small λ,

$$\frac{\partial^2 S_{\rm lin}}{\partial q_0^2}(0) = \frac{2}{\sigma^2} \frac{-Z}{\lambda} , \tag{10}$$

where Z is yet another numerical constant, and similarly for p_0, with σ replaced by $\sigma_p = \hbar/\sigma$. So the total factor resulting from the phase space integration is $\frac{\pi\hbar}{(x\lambda)} \frac{Q^2}{Z}$, again independent of σ. Combining this with the expression in Eq. (7) above, we obtain the second result, for the distribution of overlap intensities after energy and phase space averaging,

$$P(\lambda, x) = \sqrt{\frac{\pi}{2}} \frac{Q^3}{Z\sqrt{W}} \hbar\lambda (x\lambda)^{-3/2} \exp(-x\lambda/Q) . \tag{11}$$

Here we have picked up a factor of $\hbar$ from the factor of σ in Eq. (10) and the corresponding factor of $\sigma_p = \hbar/\sigma$ associated with the falloff in $S_{\rm lin}$ in the momentum direction. This indicates that the tail is coming entirely from the region near the periodic orbit, specifically from wave packets that have large classical probability density right on the orbit. (Thus, a measure like the IPR for a generically placed wave packet will not see the effect of scarring by an individual periodic orbit, when the semiclassical limit has been taken.) The result in Eq. (11) is valid in the regime

$$\max(\ln N, \lambda^{-1}) \ll x \ll N . \tag{12}$$

Here $\ln N$ is the value of x near which the RMT exponential decay law reaches values of order $\hbar = 1/2\pi N$. In this region, a crossover occurs between the head of the distribution, which is dominated by a nonscarred region of phase space and approaches the Porter-Thomas (RMT) prediction, and the tail, dominated by scarring, given by the expression above. The expression Eq. (11) holds also for an ensemble of systems, all having an orbit with instability λ. In principle, we should, of course, do a sum over all periodic orbits; however, the tail will clearly always be dominated by the orbit with the smallest λ.

Finally, we now consider an ensemble of systems where the value of the smallest exponent varies from system to system, with distribution $\mathcal{P}(\lambda) = C\lambda^\alpha$ for small λ. Then using Eq. (11) and integrating over λ we obtain

$$P(x) = C\sqrt{\frac{\pi}{2}} \frac{Q^3}{Z\sqrt{W}} Q^{\alpha+1/2} \Gamma(\alpha + 1/2) \hbar x^{-(2+\alpha)} . \tag{13}$$

Note that this is an uncontrolled approximation because we have integrated over λ after having assumed $x\lambda$ was large. However, if we had included higher-order corrections in $(x\lambda)^{-1}$ in Eq. (11), the scaling of $P(x)$ would remain unchanged, i.e.,

$$P(x) = Cf(\alpha)\hbar x^{-(2+\alpha)}, \tag{14}$$

with the dimensionless function $f(\alpha)$ somewhat different from that given in Eq. (13). An important point is that the tail displays power-law behavior in the intensity x, a strong deviation from the exponential prediction of RMT. As with Eq. (11), this asymptotic form is valid for values of x large compared to $\ln N$ and small compared to N. For small x we again expect a crossover to the Porter-Thomas form. For large x we expect a downward correction away from the $x^{-(2+\alpha)}$ form, with a breakdown of the approximation occurring at some fraction of N, depending on α.

Now, we proceed to test numerically these predictions of the nonlinear scarring theory. The system we use for this purpose is the generalized three-strip baker's map, described in some detail in [9]. This system is similar to the original baker's map, except that the two strips are replaced by three, with widths generally unequal, but normalized to $\sum_{i=0}^{2} w_i = 1$. There is a fixed point of the classical dynamics associated with the middle strip, and the instability associated with this orbit is given by $\lambda = |\ln w_1|$. So we choose $w_1 = 1/2$, set $N = 200$, and find numerically the wave function intensity distribution at the fixed point after ensemble averaging over the widths $w_{0,2}$. (The predictions are expected to hold for individual systems as well, at sufficiently large values of N. However, for the matrices which we can efficiently diagonalize, N is not large enough to obtain good statistics in the tail without ensemble averaging.) A circular wave packet of width $\sigma = \sqrt{\hbar}$ is used. The results are compared in Fig. 1 (upper thick curve) with the prediction of Eq. (7), plotted as a dashed curve. The RMT prediction is shown as a dotted line. Note that the theoretical

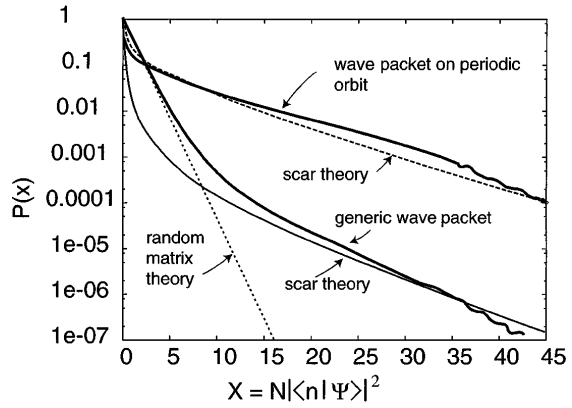

FIG. 1. Cumulative wave function intensity distribution (upper curves) as measured by a test state centered on a periodic orbit with instability $\lambda = \ln 2$, plotted as the upper thick curve with scarring theory prediction given by dashed curve, and (lower curves) averaged over the entire phase space of size $200h$, plotted as the lower thick curve with theory given by solid curve. The dotted line is the Porter-Thomas law.

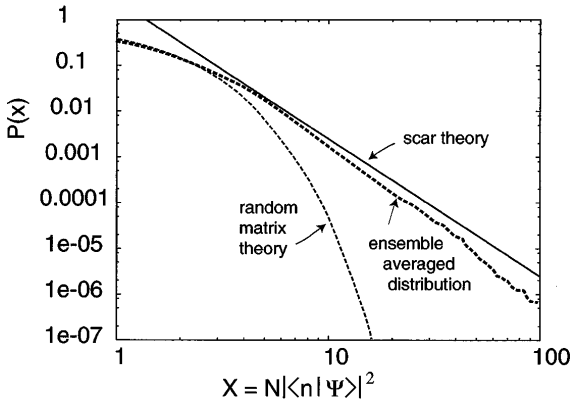

FIG. 2. Cumulative wave function intensity distribution after ensemble averaging over systems with classical orbits of different instability exponents. Here again $N = 200$, and the dotted curve is the RMT prediction.

prediction of Eq. (7) has no free parameters and is $\hbar$ independent, depending only on the exponent λ of the periodic orbit in question.

Next, we perform a phase space average for the systems described above, collecting statistics for wave packets uniformly distributed over the entire phase space. The resulting statistics are also plotted in Fig. 1 (lower thick curve), where the theoretical prediction for the tail, given by Eq. (11), is shown as a solid curve. Again, the Porter-Thomas distribution appears as a dotted line. We see a crossover between the two regimes at a value of x of order $\ln N$.

Finally, we want to construct an ensemble which will contain systems with orbits of different instability exponents λ. For this purpose, we take a uniform distribution of strip widths w_0 and w_2, each in the range $[0, 1/4]$. The fixed point in the middle strip, with exponent $\lambda = |\ln(1 - w_0 - w_2)|$, is always the least unstable periodic orbit. This ensemble has power $\alpha = 1$ and $C = 4^2 = 16$ in the notation of Eq. (13). Averaging over 100 systems, we obtain the statistics plotted in Fig. 2. The power-law prediction given by Eq. (13) is plotted as a solid line on the log-log scale, with the RMT prediction as a dotted curve. Once again, we see a crossover between the two regimes for x of order $\ln N \approx 5.3$. We also see a gradual breakdown of the approximation as x approaches values comparable to $N = 200$. Note that the quantitative agreement is in spite of the fact that an uncontrolled stationary phase approximation was used in obtaining the overall constant in front of Eq. (13), as explained above. The important thing to notice here is the power-law behavior of the tail, in agreement with the theory, and the dramatic deviation from the predictions of RMT. By $x = 100$, where the approximation $x \ll N$ is clearly beginning to break down, the measured probability is still within a factor of 4 of our prediction and is enhanced by 10^{37} over the Porter-Thomas value.

We have also checked the linear $\hbar$ dependence of the phase-space averaged results Eqs. (11) and (13) by repeating the preceding numerical analysis with larger matrices ($N = 500, 1000$). In addition, we have constructed an $\alpha = 0$ ensemble by imposing the restriction $w_0 = w_2$ and have observed a x^{-2} power-law behavior in accordance with Eq. (13).

This research was supported by the National Science Foundation under Grant No. CHE-9321260. It is a pleasure to thank E. J. Heller for many stimulating and useful discussions.

*Electronic address: kaplan@physics.harvard.edu

[1] S. Sridhar, Phys. Rev. Lett. **67**, 785 (1991).
[2] J. Stein and H.-J. Stöckman, Phys. Rev. Lett. **68**, 2867 (1992).
[3] T. M. Fromhold, P. B. Wilkinson, F. W. Sheard, L. Eaves, J. Miao, and G. Edwards, Phys. Rev. Lett. **75**, 1142 (1995); P. B. Wilkinson, T. M. Fromhold, L. Eaves, F. W. Sheard, N. Miura, and T. Takamasu, Nature (London) **380**, 608 (1996).
[4] D. Wintgen and A. Honig, Phys. Rev. Lett. **63**, 1467 (1989).
[5] K. Muller and D. Wintgen, J. Phys. B **27**, 2693 (1994).
[6] E. J. Heller, Phys. Rev. Lett. **53**, 1515 (1984).
[7] E. B. Bogomolny, Physica (Amsterdam) **31D**, 169 (1988).
[8] M. V. Berry, Proc. R. Soc. London A **243**, 219 (1989).
[9] L. Kaplan and E. J. Heller, "Linear and Nonlinear Theory of Eigenfunction Scars," Ann. Phys. (to be published).
[10] O. Agam and S. Fishman, Phys. Rev. Lett. **73**, 806 (1994); J. Phys. A **26**, 2113 (1993); O. Agam and N. Brenner, J. Phys. A **28**, 1345 (1995); S. Fishman, B. Georgeot, and R. E. Prange, J. Phys. A **29**, 919 (1996).
[11] F. P. Simonotti, E. Vergini, and M. Saraceno, Phys. Rev. E **56**, 3859 (1997); D. Klakow and U. Smilansky, J. Phys. A **29**, 3213 (1996); R. Aurich and F. Steiner, Chaos Solitons Fractals **5**, 229 (1995).
[12] V. I. Fal'ko and K. B. Efetov, J. Math. Phys. (N.Y.) **37**, 4935 (1996); K. Muller, B. Mehlig, F. Milde, and M. Schreiber, Phys. Rev. Lett. **78**, 215 (1997).